HAL open science

Multiproxy reconstruction of late quaternary upper ocean temperature in the subtropical southwestern Atlantic

Joana Cruz, Ioanna Bouloubassi, Arnaud Huguet, Alice M.S. Rodrigues, Thiago Santos, Igor Venancio, Douglas Lessa, Rodrigo Sobrinho, Rodrigo Nascimento, Marcelo Bernardes

To cite this version:

Joana Cruz, Ioanna Bouloubassi, Arnaud Huguet, Alice M.S. Rodrigues, Thiago Santos, et al.. Multiproxy reconstruction of late quaternary upper ocean temperature in the subtropical southwestern Atlantic. Quaternary Science Reviews, 2023, 307, pp.108044. 10.1016/j.quascirev.2023.108044 . hal-04150017

HAL Id: hal-04150017

https://hal.science/hal-04150017v1

Submitted on 10 Oct 2023

HAL is a multi-disciplinary open access archive for the deposit and dissemination of scientific research documents, whether they are published or not. The documents may come from teaching and research institutions in France or abroad, or from public or private research centers.

L'archive ouverte pluridisciplinaire **HAL**, est destinée au dépôt et à la diffusion de documents scientifiques de niveau recherche, publiés ou non, émanant des établissements d'enseignement et de recherche français ou étrangers, des laboratoires publics ou privés.

Manuscript File Click here to view linked References

Multiproxy reconstruction of late Quaternary upper ocean temperature in the Subtropical Southwestern Atlantic

Joana F. Cruz*[1], Ioanna Bouloubassi[2], Arnaud Huguet[3], Alice M. S. Rodrigues[1], Thiago P. Santos[1], Igor M. Venancio[1], Douglas Lessa[1], Rodrigo L. Sobrinho[1], Rodrigo A. Nascimento[1], Marcelo C. Bernardes[1]

[1]Department of Geochemistry, Federal Fluminense University, Niterói, Brazil.

[2]Laboratoire d'Océanographie et du Climat: Expérimentations et approches numériques (LOCEAN/IPSL), Sorbonne Université, Campus Pierre et Marie Curie, Paris, France.

[3]Sorbonne Université, CNRS, EPHE, PSL, UMR METIS, Paris, France.

*Corresponding author: Joana F. Cruz (joanafcruz@gmail.com)

ABSTRACT

Paleoceanographic studies addressing the oceanographic variability in the western sector of the subtropical South Atlantic - especially those focused on the Brazil Current (BC) and on a time scale that reaches marine isotope stage (MIS) 5 - are still rare when compared with equivalent studies carried out in the Northern Hemisphere. In order to close the data gap prior to the last 75 ka, in an unprecedented approach in this region, we reconstructed the upper temperature variations in the Subtropical Southwestern Atlantic (SSWA) between late MIS 6 and the onset of MIS 4 from organic proxies, using a marine sediment core (GL-1090). Sea temperature records derived from alkenone-based $U^{K'}_{37}$ and isoprenoid glycerol dialkyl glycerol tetraethers (isoGDGTs)-based TEX^{H}_{86} proxies were compared with those previously obtained from the same core via *Globigerinoides*

ruber (*G. ruber*) Mg/Ca and planktonic foraminifera Modern Analog Technique (MAT). The temporal variations of the temperature estimates derived from the $U_{37}^{K'}$ and TEX_{86}^{H} indexes showed similar patterns, even though the absolute $U_{37}^{K'}$ temperatures were systematically lower than those derived from TEX_{86}^{H}. Such a difference was related to the different habitat depths of alkenones and isoGDGTs source organisms of – haptophyte algae and marine *Thaumarchaeota*, respectively. The temperature estimates from TEX_{86}^{H} match the range of Mg/Ca and MAT-derived temperatures between 0 and 10 m depth, suggesting that these proxies reflect mixed layer temperatures. In contrast, the temperature estimates derived from $U_{37}^{K'}$ were close to the MAT values at between 0 and 100 m and to those derived from TEX_{86}^{H} between 0 and 200 m depth, demonstrating that the $U_{37}^{K'}$ proxy recorded temperatures from the upper thermocline. During MIS 5e, the difference in temperature estimates from TEX_{86}^{H} and $U_{37}^{K'}$ was reduced due to more prominent warming, probably related to a change in the thermal structure of the photic zone. Comparison of our data with studies of intensity and salinity anomalies of the Agulhas Current indicates a connection between the intensification of the Agulhas Leakage and the heat storage in the upper thermocline in the SSWA during MIS 5e. Our data suggest that the joint use of TEX_{86}^{H} and $U_{37}^{K'}$ is a promising approach to estimating paleoceanographic changes in the upper thermocline.

KEYWORDS: Alkenones; GDGTs; Subtropical Southwestern Atlantic; Last Interglacial

1. INTRODUCTION

Paleoclimate studies based on geochemical data contribute to climate modeling by providing a record of past natural climate oscillations beyond instrumental periods (Hansen et al., 2016; Otto-Bliesner et al., 2016). In this context, studies focusing on the

reconstitution of past climate variability help to understand changes that occurred in a climate similar to the present. The Marine Isotope Stage (MIS) 5e (129 - 116 thousand of years BP, hereafter – "ka"), also known as the Last Interglacial (LIG), has been widely studied in climate change investigation because it is the most recent period in which the planet was warmer than it is in the present-day and due to its similarity to the pre-industrial atmospheric greenhouse gas levels and high sea level (Turney and Jones, 2010; Capron et al., 2014; Govin et al., 2015; Otto-Bliesner et al., 2016; PAGES, 2016).

Paleoceanographic studies addressing the oceanographic variability in the western sector of the subtropical South Atlantic - especially those focused on the Brazil Current (BC) and on a time scale that reaches MIS 5 - are still rare when compared with equivalent studies conducted in the Northern Hemisphere. Most of the sea surface temperature (SST) reconstructions from the BC focus on the last 75 ka (Lourenço et al., 2016; Pereira et al., 2018; Dauner et al., 2019; Luz et al., 2020) and/or the Holocene (Pivel et al., 2013; Chiessi et al., 2014; Cordeiro et al., 2014; Evangelista et al., 2014; Lessa et al., 2014; Wainer et al., 2014; Chiessi et al., 2015; Lessa et al., 2016; Luz et al., 2020). The few temperature reconstructions for the BC that include MIS 5 were obtained from single proxies, such as planktonic foraminifera transfer function and Mg/Ca ratio (Portilho-Ramos et al., 2015; Lessa et al., 2017; Santos et al., 2017a; Santos et al., 2017b).

Since the reconstruction of sea paleotemperatures is based on proxies derived from marine organisms, SST estimates may be affected by the ecological preferences of these organisms. The most common organic geochemical proxies used to reconstruct SSTs are (i) alkenones synthesized by haptophyta algae (Brassell et al., 1986), through the $U^{K'}_{37}$ index (Prahl and Wakeham, 1987), and (ii) isoprenoid glycerol dialkyl glycerol tetraethers (isoGDGTs) from marine *Thaumarchaeota*, through the TEX_{86} index (Schouten et al., 2002). A multiproxy SST approach can help to assess the individual

proxy responses and can provide more confidence in the interpretations of how climate signals are being recorded (Mann et al., 1998; Leduc et al., 2010). Moreover, applying a multiproxy reconstruction in the same sediment core will reflect conditions from the same time period without chronological uncertainties (Huguet et al., 2011; Ausín et al., 2019).

This study is the first reconstruction of temperature variations at the upper ocean in the Subtropical Southwestern Atlantic (SSWA) using organic proxies from late -MIS 6 to the onset of MIS 4. Here, we investigated possible discrepancies in temperatures reconstructed by organic proxies, what factors may have caused such differences and we evaluated the responses of these proxies to the regional dynamics during the LIG. Sea temperatures were reconstructed from the same sediment record using the $U_{37}^{K'}$ and TEX_{86} indexes, respectively derived from alkenones and isoGDGTs. The corresponding results were compared with studies of intensity and salinity anomalies of the Agulhas Current.

2. STUDY AREA

The Santos Basin is located on the southeastern Brazilian continental margin, limited to the north by the Campos Basin and to the south by the Pelotas Basin. The upper ocean circulation (0 - 600 m) in this region is controlled by the BC, which originates from the southern branch of the South Equatorial Current (SEC) (10 – 14 °S) (Peterson and Stramma, 1991) and flows southward along the Brazilian margin (Stramma and England, 1999) (Fig. 1a). The upper layer of the BC (0 – 100 m depth) carries Tropical Water (TW) − a warm (> 20 °C), saline (> 36) and oligotrophic water mass influenced by high solar radiation, the wind field and excessive evaporation (Peterson and Stramma, 1991; Campos et al., 1995; Stramma and England, 1999; Silveira et al., 2000). The South Atlantic Central Water (SACW) corresponds to the bottom layer of the BC (100 – 600m depth; Fig. 1c) and is colder (~ 6 – 20 °C), less saline (34.6 – 36) and richer in nutrients

than the TW. The SACW flows in the thermocline layer and is formed in two sites: (i) in the Brazil-Malvinas Confluence (BMC) region, where the BC encounters the northward-flowing Malvinas Current (MC) (Peterson and Stramma, 1991) (Fig. 1a) and (ii) in the eastern region, via the Agulhas Leakage, bringing Indian Ocean Central Water into the South Atlantic (Richardson, 2007). The water masses that compose the deepest layers of the region are the Antarctic Intermediate Water (AAIW) (600 – 1200 m depth, northward direction), the Upper Circumpolar Deep Water (UCDW) (1200 – 1500 m depth, northward direction) and the North Atlantic Deep Water (NADW) (1500 – 2000 m depth, southward direction) (Stramma and England, 1999; Campos et al., 1995; Campos et al., 2000; Piola et al., 2000; Piola and Matano, 2001; Schmid, 2014; Silveira et al., 2000; Fig. 1c).

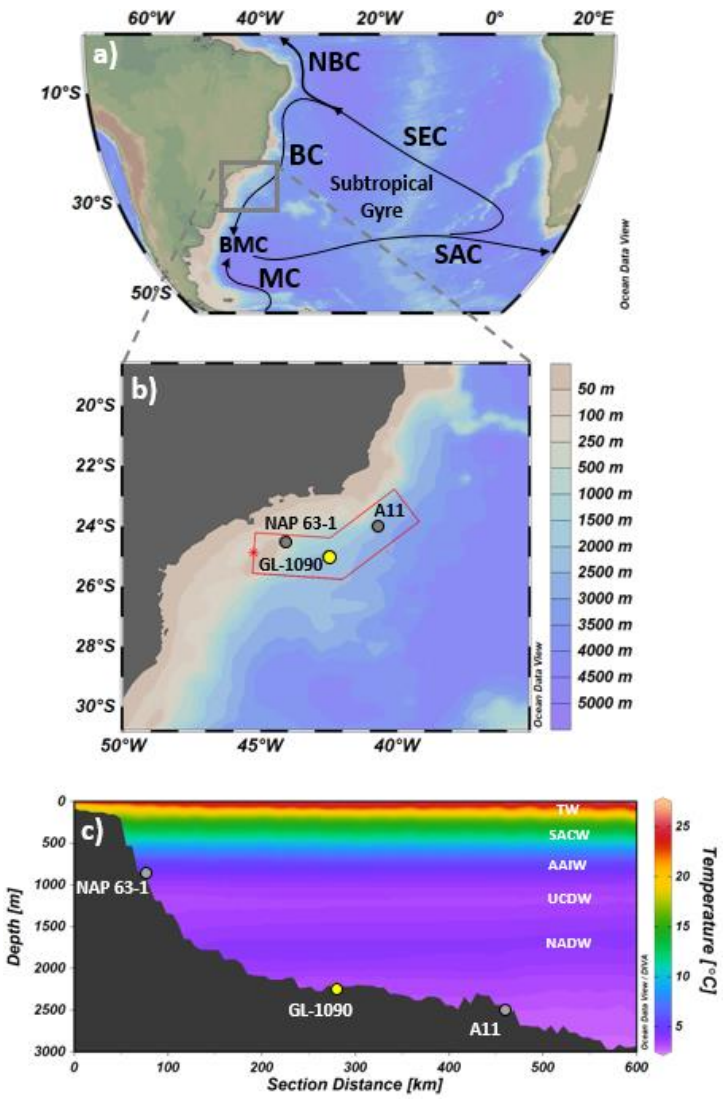

Fig. 1: Oceanographic setting of the study area and location of sediment core GL-1090. (a) South Atlantic surface circulation with the main currents of the South Atlantic subtropical gyre: (BC) Brazil Current; (BMC) Brazil-Malvinas Confluence; (MC) Malvinas (Falkland) Current; (NBC) North Brazil Current; (SAC) South Atlantic Current; and (SEC) South Equatorial Current (modified from Stramma and England, 1999). (b) Zoom of the study area (gray rectangle in a) with the position of core GL-1090 (this study) and cores used in the discussion: downcore NAP63-1 (Dauner et al., 2019) and core-top A11 (Ceccopieri et al., 2018). (c) Vertical section of the first 3000 m water depth of the Santos Basin (highlighted red section in b) showing the cores mentioned above and the water masses that compose the region: (TW) Tropical Water, (SACW) South Atlantic

Central Water, (AAIW) Antarctic Intermediate Water; (UCDW) Upper Circumpolar Deep Water and (NADW) North Atlantic Deep Water. This figure was partly created with the software Ocean Data View (Schlitzer, 2003). (For interpretation of the references to color in this figure legend, the reader is referred to the web version of this article.)

Instrumental data show that the annual mean SST of the TW (0 m depth) is 24 °C, with the lowest SST (22.2 °C) during austral winter and the highest SST (25.8 °C) during austral summer (Locarnini et al., 2013). The difference in temperature between summer and winter is most pronounced in the upper 20 m of the water column (Fig. 2).

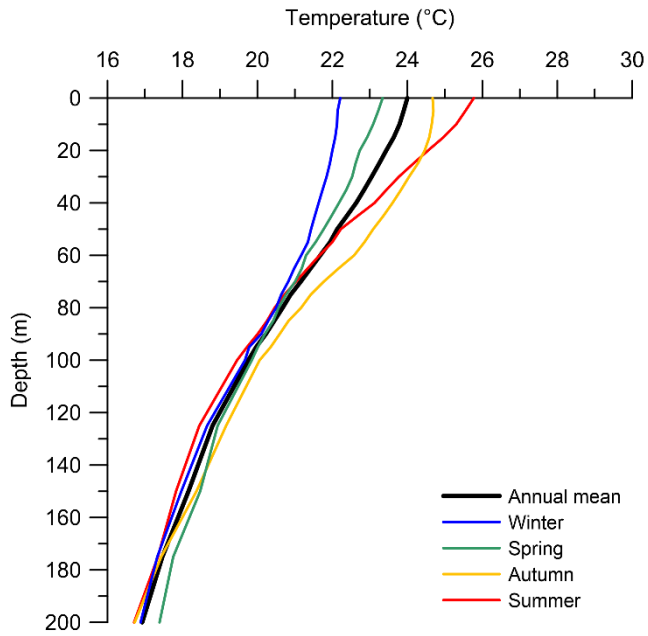

Fig. 2: Vertical profiles of the present-day temperatures in the upper 200 m of the study area provided by the World Ocean Atlas 2013 (Locarnini et al., 2013): annual mean (black), winter (blue), spring (green), autumn (yellow) and summer (red). (For interpretation of the references to color in this figure legend, the reader is referred to the web version of this article.)

3. MATERIAL AND METHODS

3.1. Sediment sampling and age model

The marine sediment core GL-1090 (24.92 °S, 42.51 °W, 2225 m water depth, 1914 cm length) was collected by Petrobras on the continental slope of the Santos Basin (Fig. 1) and stored in a refrigerated container at 4 °C. The age model, shown for the first time in Santos et al. (2017a), was based on radiocarbon dating and visual alignment of $\delta^{18}O$ from benthic foraminifera with two reference curves, MD95-4042 (Govin et al., 2014) and LR04 $\delta^{18}O$ global stack (Lisiecki and Raymo, 2005). The final age model was built using Bacon software v.2.2 (Blaauw and Christeny, 2011). Recently, Ballalai et al. (2019) and Santos et al. (2020) implemented several improvements over the original age model. Ballalai et al. (2019) chose one of the 230^{Th} ages of the Sanbao cave as the connection point for the abrupt transition observed in the corrected ice volume $\delta^{18}O$ at the end of Termination II. This modification, with assumes a coupling between the movements of the Intertropical Convergence Zone and the bifurcation of the South Equatorial Current in the tropical Atlantic, reduced age uncertainties from ± 3.87 to ± 1.51 ka close to the transition to the LIG. Santos et al. (2020) derived more benthic $\delta^{18}O$ tie- points between GL-1090 and the Iberian Margin MD95-2042 (Govin et al., 2014) on the AICC2012 time scale (Bazin et al., 2013; Veres et al., 2013). The success of the new tie-points can be seen through a precise alignment between the variability on the $\delta^{18}O$ millennial scale of *Globorotalia inflata* and NGRIP (Santos et al., 2020). Core GL-1090 spans the last 185 ka. This study is focused on the age interval from 150 to 65 ka, corresponding to the depth interval from 1591 to 689 cm. Each subsample is 2 cm thick with average collection intervals of 5 cm, corresponding to an average sampling resolution of approximately 400 years.

3.2. Lipid biomarker extraction and fractionation

Lipids were extracted from dry-frozen sediments (2 - 5 g) via three ultrasonication cycles using a solvent mixture of dichloromethane/methanol, 3:1 (v:v). The total lipid extracts were further separated into three fractions by silica gel chromatography using solvent mixtures of increasing polarity: 4 mL of hexane (elution of *n*-alkanes - not discussed in this study); 2 mL of hexane/ethyl acetate 95:5 (v:v) and then, in sequence, 2 mL of hexane/ethyl acetate 90:10 (v:v) (elution of alkenones); and 5 mL of hexane/ethyl acetate 70:30 (v:v) (elution of GDGTs).

3.3. Alkenone analysis and temperature estimations

The fractions containing alkenones were analyzed on an Agilent 6890 Plus gas chromatograph coupled with a flame ionization detector (GC-FID), and equipped with a CPSIL-5 CB column (50 m long × 0.32 mm internal diameter × 0.25 μm film thickness). Helium gas was used as carrier gas (2.0 mL/min). The oven was programmed with an initial temperature of 50 °C, which was then increased to 140 °C at 30 °C/min, then to 280 °C at 20 °C/min, and finally to 305 °C at 0.5 °C/min. Di- and tri-unsaturated C_{37} alkenones ($C_{37:2}$ and $C_{37:3}$, respectively) were quantified by comparing their peak area with that of an internal standard (5α-cholestane, added prior to analysis).

The alkenone unsaturation index $U_{37}^{K'}$ was calculated according to Prahl and Wakeham (1987; Equation 1) and converted into temperature values using the Bayesian B-spline regression model, BAYSPLINE, for the $U_{37}^{K'}$ paleothermometer (Tierney and Tingley, 2018), with a standard error of ± 1.0 °C.

$$U_{37}^{K'} = \frac{C_{37:2}}{C_{37:2} + C_{37:3}} \quad (1)$$

3.4. GDGT analysis and temperature estimations

GDGT analyses were performed on a Shimadzu LCMS-2020 high-performance liquid chromatography-mass spectrometry (HPLC-MS) system, as recently described by Huguet et al. (2019). The semi-quantification of the GDGTs was performed by comparing the peak area of the internal standard C_{46}GDGT with those of the compounds (cf. Huguet et al., 2013).

The TEX_{86} index was calculated according to Schouten et al. (2002) (Equation 2). The numbering of the isoGDGTs refers to the publication by Kim et al. (2010).

$$TEX_{86} = \frac{\text{isoGDGT-2 + isoGDGT-3 + Crenarchaeol regioisomer}}{\text{isoGDGT-1 + isoGDGT-2 + isoGDGT-3 + Crenarchaeol regioisomer}} \quad (2)$$

The annual mean sea surface temperatures (0 m) were estimated from the TEX_{86}^{H} index (Equation 3) using the calibration by Kim et al. (2010) adapted for temperatures between 15 – 30 °C, with a given uncertainty of ± 2.5 °C (Equation 4).

$$TEX_{86}^{H} = \log(TEX_{86}) \quad (3)$$

$$\text{Temp-}TEX_{86}^{H}\ (°C) = 68.4\ (TEX_{86}^{H}) + 38.6 \quad (4)$$

The annual mean depth-integrated temperatures (0 to 200m water depth) were calculated from the global calibration by Kim et al. (2012; Equation 5), with an uncertainty of ± 2.2 °C.

$$\text{Temp-}TEX_{86}^{H}(0\text{-}200)\ (°C) = 54.7\ (\ TEX_{86}^{H}) + 30.7 \quad (5)$$

The Branched and Isoprenoid Tetraether (BIT) index is suggested to represent terrestrial organic matter inputs into aquatic environments (Hopmans et al., 2004). In order to evaluate if TEX_{86}^{H} values were biased by terrigenous input at our core site, the BIT index was calculated from Hopmans et al. (2004) (Equation 6). The numbering of the branched GDGTs (brGDGTs) refer to the publication by Hopmans et al. (2004). High BIT values (> 0.4) may lead to anomalously high TEX_{86}^{H}-derived temperatures (Weijers et al., 2006).

$$\text{BIT index} = \frac{\text{brGDGT-I} + \text{brGDGT-II} + \text{brGDGT-III}}{\text{brGDGT-I} + \text{brGDGT-II} + \text{brGDGT-III} + \text{Crenarchaeol}} \quad (6)$$

4. RESULTS

4.1. Alkenone-derived temperatures (Temp-$U_{37}^{K'}$)

During the period between 150 and 65 ka, the mean Temp-$U_{37}^{K'}$ was 20.8 °C ± 1.4 and ranged from 17.6 °C (ca. 146.4 ka ka, MIS 6) to 26.8 °C (ca. 126.6 ka, MIS 5e) (Fig. 3a). The alkenone temperature estimates were mainly below the mean value from 150 to 140 ka (MIS 6 / T II). An abrupt warming of 6.1 °C marked the Termination II (T II), reaching a peak during MIS 5e (~127 ka), followed by a gradual cooling until mid-MIS 5d (ca. 112 ka). The MIS 5e, 5c, and 5a substages generally showed warmer temperatures than MIS 5d and 5b substages. The periods between ca. 82 - 79 ka and ca. 77 - 75 ka were marked by a decrease in temperature.

4.2. GDGT-derived temperatures (Temp-TEX_{86}^{H}, Temp-TEX_{86}^{H} (0-200)

The mean Temp-TEX_{86}^{H} from 140 to 65 ka was 25.4 ºC ± 1.4, ranging from 21.1 ºC (ca. 68.4 ka, MIS 4) to 28.5 ºC (ca. 123.8 ka, MIS 5e) (Fig. 3a). The T II was marked by an abrupt warming of 5.7 °C. Throughout the substages MIS 5d to MIS 5a, the

temperatures remained roughly stable, except for two abrupt decreases in temperature during MIS 5a. The minimum temperature was recorded at the MIS 5a / 4 (21.1 °C at 69 ka). Regarding the depth-integrated temperatures, Temp-TEX_{86}^{H} (0-200) oscillated between 16.7 ºC (ca. 68.4 ka, MIS 4) and 22.7 ºC (ca. 123.8 ka, MIS 5e), with an average of 20.1 ºC ± 1.2 (Fig. 4).

5. DISCUSSION

5.1. Comparison of the TEX_{86}^{H} and $U_{37}^{K'}$ temperature estimates

In core GL-1090, similar trends were generally observed for temperatures derived from alkenones and isoprenoid GDGTs (Temp-$U_{37}^{K'}$ and Temp-TEX_{86}^{H}), with a high amplitude during LIG (Fig. 3). Nevertheless, the two organic proxies provided different absolute temperature estimates. $U_{37}^{K'}$-derived temperatures were systematically lower than those provided by TEX_{86}^{H} (Fig. 3a). The peaks of Temp-$U_{37}^{K'}$ and Temp-TEX_{86}^{H} were 26.8 °C (126.6 ka, MIS 5e) and 28.5 °C (123.8 ka, MIS 5e), respectively, which are 2.8 °C and 4.5 °C higher than the current annual mean surface temperature (0 m depth) near the GL-1090 site (Fig. 3a).

Turney and Jones (2010) compiled a global dataset of annual temperatures from cores spanning the LIG and deduced an increase in sea surface and terrestrial temperatures of nearly 2.0 °C above pre-industrial levels over this period. However, such warming was not uniform across the global oceans, and the SSWA was not included in the dataset. Model data performed by Otto-Bliesner et al. (2013) and sea surface temperature reconstructions published by Hoffman et al. (2017) did not indicate a significant difference in temperature during the LIG compared with the present in global tropical regions. It should be noted that these authors did not present results near our sampling site.

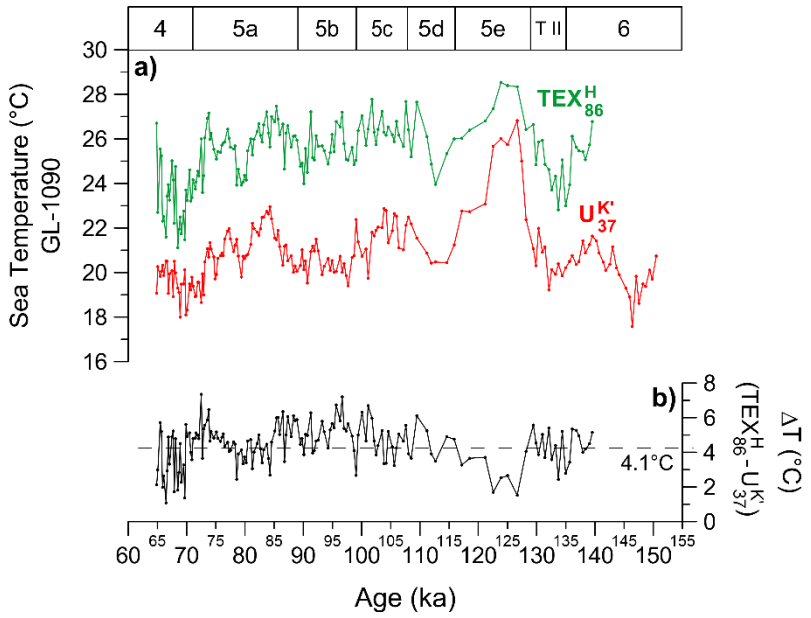

Fig. 3: Comparison of paleotemperatures reconstructed from isoGDGTs and alkenones: a) Temp-TEX^{H}_{86} (green) and Temp-$U^{K'}_{37}$ (red). The dashed line in violet marks the global average increase during the LIG, approximately 2.0 °C relative to pre-industrial levels (Turney and Jones, 2010). The blue dashed line marks the current annual mean sea surface temperature in the study area (Locarnini et al., 2013); b) Temperature gradient ΔT (TEX^{H}_{86} - $U^{K'}_{37}$). The black dashed line marks the average ΔT (4.1 °C). The marine isotopic stages (MIS) are highlighted on the upper x-axis. (For interpretation of the references to color in this figure legend, the reader is referred to the web version of this article.)

The peak of Temp-$U^{K'}_{37}$ from GL-1090 is consistent with the + 2.0 °C LIG surface temperature anomaly relative to the present-day mean (Turney and Jones, 2010), equivalent to 24 °C in the study area (Cordeiro et al., 2014; Locarnini et al., 2013). In contrast, Temp-TEX^{H}_{86} showed a very high LIG SST anomaly relative to the modern annual mean (4.5 °C), which does not seem plausible. In order to understand the similarities and divergences between the temperature estimates derived from $U^{K'}_{37}$ and

TEX_{86}^{H}, the different factors which may influence these organic proxies and their associated temperatures – choice of calibration equations, continental inputs, lateral transport of the alkenones and isoGDGTs, ecology and seasonality of the source organisms of these lipids – will be considered in detail below.

5.2. Potential factors influencing the $U_{37}^{K'}$ and TEX_{86}^{H} temperature estimates

5.2.1. Choice of the calibrations

The choice of the calibration has an influence on the absolute temperature estimates. We tested the Temp-$U_{37}^{K'}$ annual calibration for the global ocean from 60 °N to 60 °S (Müller et al., 1998), the Temp-$U_{37}^{K'}$ SE Atlantic annual mean core top calibration (Müller et al., 1998) and the new Bayesian B-spline regression model, BAYSPLINE, for the $U_{37}^{K'}$ paleothermometer (Tierney and Tingley, 2018). The three calibrations resulted in highly similar temperatures (cf. Supp. Fig. 1). The annual calibration for the global ocean from 60 °N to 60 °S resulted in Temp-$U_{37}^{K'}$ on average 0.8 °C warmer than the values obtained with the SE Atlantic annual calibration equation proposed by Müller et al. (1998). The Temp-$U_{37}^{K'}$ calibration by Tierney and Tingley (2018) resulted in Temp-$U_{37}^{K'}$ on average 0.04 °C warmer than the values calculated with the SE Atlantic annual calibration equation proposed by Müller et al. (1998).

Using 53 core-top sediments, Ceccopieri et al. (2018) tested on a regional scale in the SSWA (SE Brazilian continental margin) the applicability of Temp-$U_{37}^{K'}$ calibrations by Müller et al. (1998) for the SE Atlantic: annual mean core top calibration (for temperatures from 0 to 27 °C) and seasonal (austral) calibrations. These authors concluded that the Temp-$U_{37}^{K'}$ SE Atlantic annual calibration (Müller et al., 1998) is comparable to SSWA annual mean present-day temperatures. Due to the high similarity between the Temp-$U_{37}^{K'}$ SE Atlantic annual mean core top calibration (Müller et al., 1998)

and Temp-$U^{K'}_{37}$ calibration by Tierney and Tingley (2018), both calibrations could be used interchangeably. In this work we adopt the most recent one.

Regarding GDGTs, we tested the Temp-TEX^{H}_{86} calibration proposed by Kim et al. (2010), the Temp-TEX^{H}_{86}(0-200) calibration by Kim et al. (2012), and the Temp-TEX^{H}_{86} and Temp-TEX^{H}_{86}(0-200) calibrations by Tierney and Tingley (2014). The TEX^{H}_{86} and TEX^{H}_{86} (0-200) calibrations by Tierney and Tingley (2014) resulted in a less pronounced temperature oscillation over time, and the absolute surface and subsurface values were closer to each other (cf. Supp. Fig. 2). The TEX^{H}_{86} calibration by Tierney and Tingley (2014) resulted in colder absolute temperatures than the TEX^{H}_{86} calibration by Kim et al. (2010). The TEX^{H}_{86} (0-200) calibration by Tierney and Tingley (2014) resulted in warmer absolute temperatures than the TEX^{H}_{86} (0-200) calibration by Kim et al. (2012).

The applicability of the Temp-TEX^{H}_{86} calibration for regions with present-day temperatures from 15 to 30 °C proposed by Kim et al. (2010) was also tested by Ceccopieri et al. (2018) in the SSWA using the same core-top sediments as for the $U^{K'}_{37}$ investigation. Temp-TEX^{H}_{86} was found to reflect the annual temperature in the SSWA. Although the Temp-TEX^{H}_{86} by Tierney and Tingley (2014) are closer to the present-day temperature in GL-1090, we adopted Kim et al. (2010) calibration because its regional application in our study area was already validated by previous study.

5.2.2. Continental inputs

Temp-TEX^{H}_{86} may be biased by isoprenoid GDGTs derived from terrigenous inputs and transported to the marine system by rivers and/or runoff (Schouten et al., 2013 and references therein). These inputs can notably be quantified by applying the BIT index (Hopmans et al., 2004), whose values close to 0 were generally associated with organic

material from open sea origin and those close to 1 (maximum value) with organic matter from terrestrial origin. In marine settings, BIT values above 0.4 were suggested to cause a deviation of the TEX_{86} temperature estimates greater than 2.0 °C (Weijers et al., 2006). Nevertheless, care should be taken when interpreting the BIT values, as the two types of GDGTs used to calculate the BIT index - branched glycerol dialkyl glycerol tetraethers (brGDGTs) (Peterse et al., 2009; Sinninghe Damsté et al., 2009; Tierney et al., 2010) and crenarchaeol (Leininger et al., 2006; Weijers et al., 2006; Walsh et al., 2008) - can be produced in both terrestrial and aquatic environments. Therefore, in aquatic settings, high BIT values, which reflect a higher relative abundance of brGDGTs than that of crenarchaeol, could be associated with high terrestrial inputs of brGDGTs and/or *in situ* production of brGDGTs.

Along the core GL-1090, the BIT index varied between 0.11 and 0.92, with an average of 0.45 ± 0.12 and higher values recorded during cold periods, from late MIS 6 to the onset of MIS 5e and during the onset of MIS 4 (cf. Supp. Fig. 3). Considering that previous studies have shown that no large river flows directly to the sea in this region (Conti and Furtado, 2006; Pessenda et al., 2012), terrestrial inputs were not expected to be high in the study area. To better evaluate this hypothesis, the behavior of organic and inorganic compounds from the same core was investigated, even though the latter are transported from the continent to marine sediments by different particles. No similar trends were observed between the BIT values and the Fe/Ca ratio - an inorganic proxy from continental runoff along the GL-1090 core (Figueiredo et al., 2020). The Fe/Ca peaks were not even registered by the BIT index or by Temp-TEX_{86}^{H} (cf. Supp. Fig. 3).

However, the calcium ratios are influenced by sea level in the study area, embedding a very dominant low-frequency variability in the data. This sea level influence may suggest that the null correlation between BIT and XRF may not be substantially strong

evidence. Recently, Mathias et al. (2021) performed a deep sedimentological analysis on GL-1090 and they found very little river entry into the continental margin of southeastern Brazil during the Late Pleistocene. Although there was some continental influence, the results indicated the lowest terrigenous entries during MIS 5e and MIS 1. This suggests that the BIT values cannot be interpreted as recording high terrestrial inputs, since its highest values were found during MIS 5e. The high BIT values would rather be due to *in situ* production of brGDGTs at the GL-1090 sampling site, as observed in coastal regions (Crampton-Flood et al., 2019).

5.2.3. Lateral transport

The effect of lateral transport on $U_{37}^{K'}$ temperature estimates has been reported in specific oceanic regions. Anomalously cold (by 2 °C – 6 °C) $U_{37}^{K'}$ temperature values were found in sediments located under the Brazil–Malvinas Confluence and Malvinas Current in the southwestern Atlantic (Benthien and Muller, 2000). In this area of peculiar circulation, alkenone-bearing sediments are advected northwards carrying $U_{37}^{K'}$ signals of their origin in cold waters. In the Campos Basin, SSWA, cold bias in Uk'37 derived temperatures wre reported in core-top sediments close to the Cabo Frio Upwelling System and they were ascribed to alkenones advected from adjacent colder (upwelled) waters.

Considering that alkenones are more susceptible to lateral transport than isoGDGTs (Mollenhauer et al., 2007; Shah et al., 2008), Ceccopieri et al. (2018) suggested that TEX_{86}^{H}–derived estimates better reflect local temperatures in this region in comparison with alkenones. In line with the conclusion of Ceccopieri et al. (2018), the lower absolute values of $U_{37}^{K'}$ compared with those of TEX_{86}^{H} could be explained by intrusions of SACW into the photic zone identified in the GL-1090 during MIS 5e, 5c, and 5a substages due to the southward expansion of the Cabo Frio Upwelling System (Lessa et al. 2017).

Nevertheless, it should be noted that, while Lessa et al (2017) showed a vertical cooling only during warm substages, here Temp-$U^{K'}_{37}$ presented lower values than Temp-TEX^{H}_{86} during the entire studied period (150 – 65 ka), indicating that the advection of cold water alone cannot explain the differences in TEX^{H}_{86} and $U^{K'}_{37}$-based temperature estimates. Additionally, the similar pattern and the high correlation between temperatures derived from the $U^{K'}_{37}$ and TEX^{H}_{86} indices ($r = 0.73$, $p < 0.05$) suggest that either (i) the signals from the alkenones and isoGDGTs were produced vertically in the same area, probably at different depths in the water column, or (ii) the intensity of the lateral transport might differ over the investigated period, affecting both types of lipids in the same way during some periods. In any case, it means that lateral transport alone cannot explain the differences in absolute temperatures between $U^{K'}_{37}$ and TEX^{H}_{86}.

5.2.4. Seasonality

In a number of studies disparities between paleotemperatures reconstructed with the $U^{K'}_{37}$ and TEX^{H}_{86} indexes have been attributed to seasonal patterns in the production of the organisms, hapophyte algae and marine Thaumarchaeota, respectively (eg Lopes dos Santos et al., 2013; Auderset et al., 2019) but a consistent, globally applicable, seasonal pattern has not emerged.

Furthermore, compilation of sediment trap time series data have shown that the maximum alkenone flux across the oceans displays seasonal variations depending on local/regional oceanographic conditions and sedimentation processes (Mele and Prahl 2013). However, apart from few locations close to major hydrographic fronts, sedimentation patterns for $U^{K'}_{37}$ in sediment trap time series appears provide a measure of annual mean SST.

The age of the GL-1090 core-top sample is 6.6 ka (Santos et al., 2017a), hampering its use to compare the seasonality of alkenone and isoGDGT source organisms - hapophyte algae and marine *Thaumarchaeota*, respectively - in the present-day. However, core-top studies in the SSWA shelf and slope (Cordeiro et al., 2014; Ceccopieri et al., 2018) have found that $U_{37}^{K'}$-derived temperature estimates agreed well with interpolated mean annual SST of ca. 24 °C. They also reported that, despite a likely most efficient export of isoGDGT during austral summer, core-top Temp-TEX_{86}^{H} values were better correlated with the annual mean SST (Ceccopieri et al., 2018). In the regional context, Mahiques et al. (2005) analyzed alkenones in box cores near GL-1090 and considered Temp-$U_{37}^{K'}$ as reflecting mean annual temperatures over the last 700 years. A similar conclusion was drawn by Dauner et al. (2019), who showed that the temperature estimates derived from TEX_{86}^{H} and $U_{37}^{K'}$ over the last 75 ka reflected the mean annual temperature in the SSWA.

Based on the afore-mentioned studies we argue that seasonal bias in the Temp-TEX_{86}^{H} and Temp-$U_{37}^{K'}$ estimates is of minor importance and that both TEX_{86}^{H} and $U_{37}^{K'}$ indexes record the mean annual temperature in the study area.

5.2.5. Water depth

Standard deviations of ± 1.0 °C for Temp-$U_{37}^{K'}$ (Müller et al., 1998) and ± 2.5 °C for Temp-TEX_{86}^{H} (Kim et al., 2010) suggest that temperature differences of up to ± 3.5 °C between these proxies may be within the calibration error. The reconstructed mean temperature gradient (ΔT) of TEX_{86}^{H} and $U_{37}^{K'}$ is 4.5 °C (Fig. 3b) and, therefore, higher than the calibration error. One explanation may be the difference of depth production between haptophytes and *Thaumarchaeota*.

Previous studies at the Campos Basin slope indicate that haptophyte algae, alkenone producers, inhabit the photic zone between 6 – 50 m depth (predominantly the 20 °C isotherm; Mahiques et al., 2009; Sousa et al., 2014; Rodrigues et al., 2014). This temperature isotherm corresponds to the interface between TW and SACW at the Santos Basin slope. Dauner et al. (2019) concluded that the temperatures derived from $U_{37}^{K'}$ were consistent with those at around 30 m depth in the SSWA. Similarly, Luz (2019) considered that the $U_{37}^{K'}$ signal reflected the temperature of the water column up to 25 m in the same region. This is consistent with previous studies in other areas, such as the Mediterranean Sea, the northern Arabian Sea, and in the tropical and subtropical Atlantic Ocean, which reported the possibility of alkenones recording temperature conditions below the surface (Ternois et al., 1997; Andruleit et al., 2003; Poulton et al., 2017).

IsoGDGT-producing archea are generally more widely distributed in the water column than haptophytes, presenting a greater abundance between 40 and 150 m water depth (Lopes dos Santos et al., 2013; Kim et al., 2012; Schouten et al., 2002; Wuchter et al., 2006). In their study of the structure of the picoplankton community in a southern Atlantic transect, Zubkov et al. (2000) indicated that heterotrophic prokaryotes (bacteria and archea) mainly inhabit the surface layer. While Dauner et al. (2019) confirmed that the TEX_{86}^{H} signal represents the average annual temperature of the surface layer at the Santos Basin, Luz (2019) considered that Temp-TEX_{86}^{H} reflects those of the water depths around 100 - 200m, showing that there is no consensus on the depth of *Thaumarchaeota* growth in the SSWA.

Assuming that the non-thermal factors investigated in the previous sections (5.2.1, 5.2.2, 5.2.3 and 5.2.4) do not cause significant deviations in temperature reconstructions, the results for the GL-1090 core suggest that the alkenones reflect temperatures at the

interface between the TW and the SACW, corresponding to the upper thermocline, and the isoGDGTs reflect temperatures at the mixed layer of the Santos Basin slope.

5.3. Multiproxy temperature reconstruction in the water column

In order to estimate the temperature gradient (ΔT) between the mixed layer and the upper thermocline from GL-1090, Temp-TEX_{86}^{H}(0-200) – for subsurface temperature – was calculated and compared with Temp-TEX_{86}^{H} – for surface temperature. The average ΔT between Temp-TEX_{86}^{H} and Temp-TEX_{86}^{H}(0-200) was 5.2 °C (Fig. 4a), while the average ΔT between Temp-TEX_{86}^{H}(0-200) and Temp-$U_{37}^{K'}$ was considerably smaller (less than 1.0 °C) (Fig. 4b).

Ceccopieri et al. (2018) also applied the Temp-TEX_{86}^{H}(0-200) calibration by Kim et al. (2012) to core-top samples. At station A11 (Fig. 1b,c), these authors obtained values close to instrumental data from WOA13 (Locarnini et al., 2013) depth-integrated temperatures at about 100 - 200 m depth throughout the Campos Basin slope (between 13.8 °C and 21.7 °C). This suggests that the $U_{37}^{K'}$ signal at the GL-1090 site reflects the upper thermocline temperature in the SSWA.

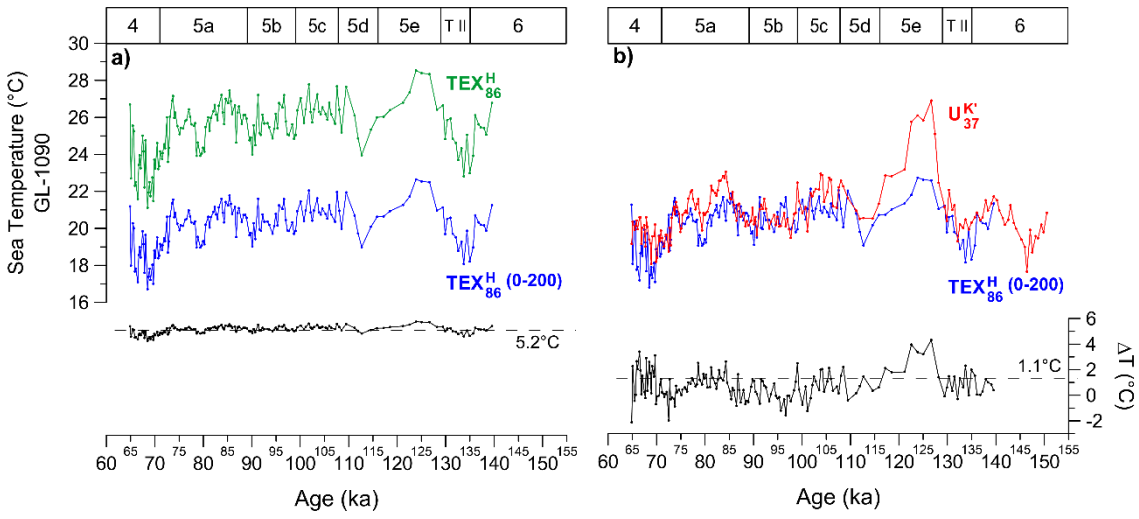

Fig. 4: Comparison of depth-integrated TEX_{86}^{H}(0-200) with TEX_{86}^{H} and $U_{37}^{K'}$-based temperatures, and their respective temperature gradients: a) TEX_{86}^{H} (green), TEX_{86}^{H}(0-200) (blue) and ΔT (TEX_{86}^{H}-TEX_{86}^{H}(0-200)) (black); b) $U_{37}^{K'}$ (red), TEX_{86}^{H}(0-200) (blue) and ΔT ($U_{37}^{K'}$-TEX_{86}^{H}(0-200)) (black). Dashed lines mark the mean difference between the absolute temperatures derived from the organic proxies. Marine isotope stages (MIS) are highlighted on the upper x-axis. (For interpretation of the references to color in this figure legend, the reader is referred to the web version of this article.)

The sea temperature estimates derived from $U_{37}^{K'}$ and TEX_{86}^{H} were compared with those inferred for the same core from Mg/Ca *G. ruber* (Santos et al., 2017a) and from Modern Analog Technique (MAT) - a transfer function based on planktonic foraminiferal census count (Lessa et al., 2017) - at 10m (MAT-10m) and at 100m (MAT-100m) water depth. The Mg/Ca values published in Santos et al. (2017a) were converted to temperatures using the recent species-specific equation by Gray and Evans (2019). The calcification depth of *G. ruber* in the SSWA corresponds to the mixed layer (30 – 40m water depth), as shown by sediment traps studies (Venancio et al., 2017). This supports the use of the Mg/Ca proxy for reconstructing mixed layer temperatures in the region (eg Chiessi et al., 2007; Chiessi et al. 2014). Temp-TEX_{86}^{H} values fall into the range of those derived from Mg/Ca and are close to MAT-10m temperatures, suggesting that these proxies reflect mixed layer temperatures (Fig. 5a).

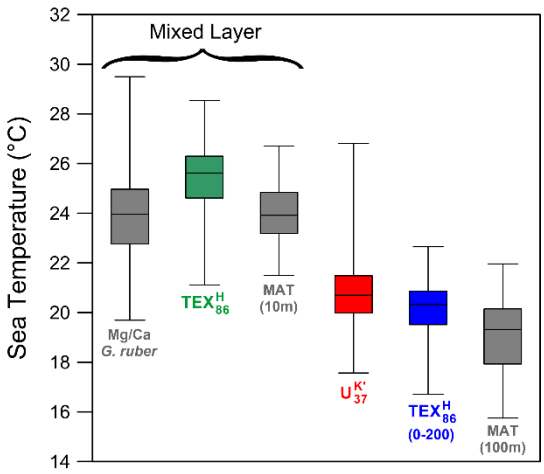

Fig. 5: Comparison of paleotemperature ranges reconstructed from multiproxies at GL-1090, between 150 and 65 ka: temperature (°C) derived from Mg/Ca *G. ruber* (gray) (after Santos et al., 2017a); TEX^{H}_{86} (green) (this study); MAT-10m (gray) (Lessa et al., 2017); $U^{K'}_{37}$ (red) (this study); TEX^{H}_{86}(0-200) (blue) (this study); and MAT-100m (gray) (Lessa et al., 2017). (For interpretation of the references to color in this figure legend, the reader is referred to the web version of this article.)

In contrast, the range of temperatures derived from $U^{K'}_{37}$ is similar to the ones from TEX^{H}_{86}(0-200) and MAT-100 m. The corresponding estimates are lower than Mg/Ca, TEX^{H}_{86} and MAT-10m-based temperatures, suggesting that, in core GL-1090, Temp-$U^{K'}_{37}$ recorded temperatures from the upper thermocline. This is consistent with the fact that, in the SSWA, haptophytes reach their maximum abundance where the deep chlorophyll maximum occurs, above the thermocline (Brandini et al., 2014; Rodrigues et al., 2014; Ribeiro et al., 2016). Dauner et al. (2019) also attributed to the depth of the haptophyte habitat the lower Temp-$U^{K'}_{37}$ than Temp-TEX^{H}_{86} over the last 75 ka in the SSWA, and this condition seems to be the most likely to explain why the temperatures derived from $U^{K'}_{37}$ are more similar to the temperatures from the upper thermocline than from the mixed layer in GL-1090, between 150 and 65 ka (Fig. 5b).

5.4. Regional dynamics in the water column in the SSWA during MIS 5e

During the MIS 5e (129-116 ka) and the onset of MIS 4 (71-65 ka), the ΔT between TEX_{86}^{H} and $U_{37}^{K'}$ was lower than the average one over the whole core GL-1090 (Fig. 3b). During the MIS 5e, the ΔT was reduced due to a more prominent warming of $U_{37}^{K'}$. In contrast, during the onset of the MIS 4, this decrease could be explained by a more pronounced cooling of TEX_{86}^{H}. If we assume that the source organisms of alkenones and isoGDGTs live at different depths, then a change in the thermal structure of the photic zone may explain the similar temperatures between the mixed layers and the upper thermocline during MIS 5e and the onset of MIS 4. The pronounced positive temperature anomaly derived from $U_{37}^{K'}$ during MIS 5e (Fig. 6a) suggests greater heat storage at the upper thermocline.

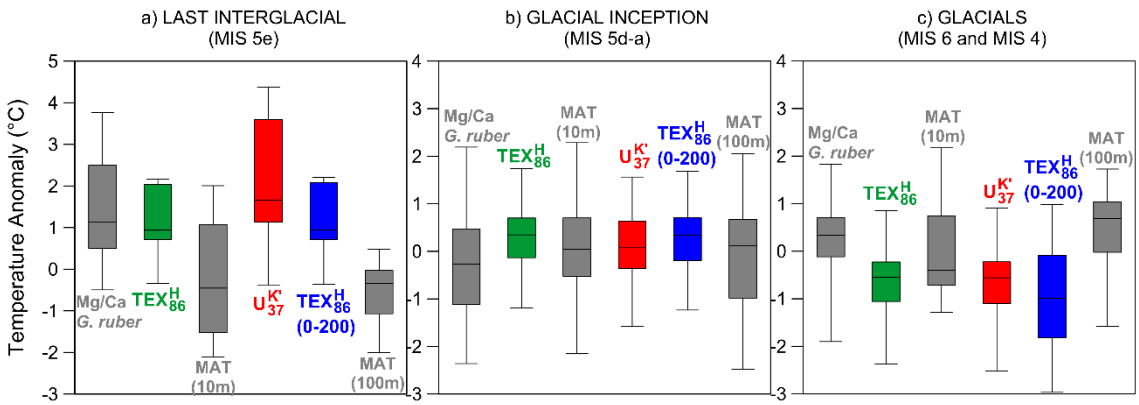

Fig. 6: Temperature anomalies normalized by the standard deviation of each proxy along the core GL-1090 for three time intervals: (a) Last Interglacial (LIG/MIS 5e); (b) Glacial inception (MIS 5d-a); (c) Glacials (MIS 6 and MIS 4), based on Mg/Ca *G. ruber* (gray) (after Santos et al., 2017a); TEX_{86}^{H} (green) (this study); MAT-10m (gray) (Lessa et al., 2017); $U_{37}^{K'}$ (red) (this study); TEX_{86}^{H}(0-200) (blue) (this study); and MAT-100m (gray)

(Lessa et al., 2017). (For interpretation of the references to color in this figure legend, the reader is referred to the web version of this article.)

During the LIG period (Figure 6a), $U_{37}^{K'}$ recorded a steep thermal gradient in the upper thermocline, which decreased in the middle/end of the interglacial complex scenario (Figure 6b). The intensity of this thermal gradient was further reduced in the glacial scenario (Figure 6c). The evaluation of these different water column temperature profiles over time suggests that alkenones are more strongly affected by changes in depth conditions than isoGDGTs, the latter being directly affected by the vertical mixing temperature oscillation. This explains why $U_{37}^{K'}$-based temperatures are similar to those of the surface layer during the LIG and close to the subsurface temperatures during the glacials.

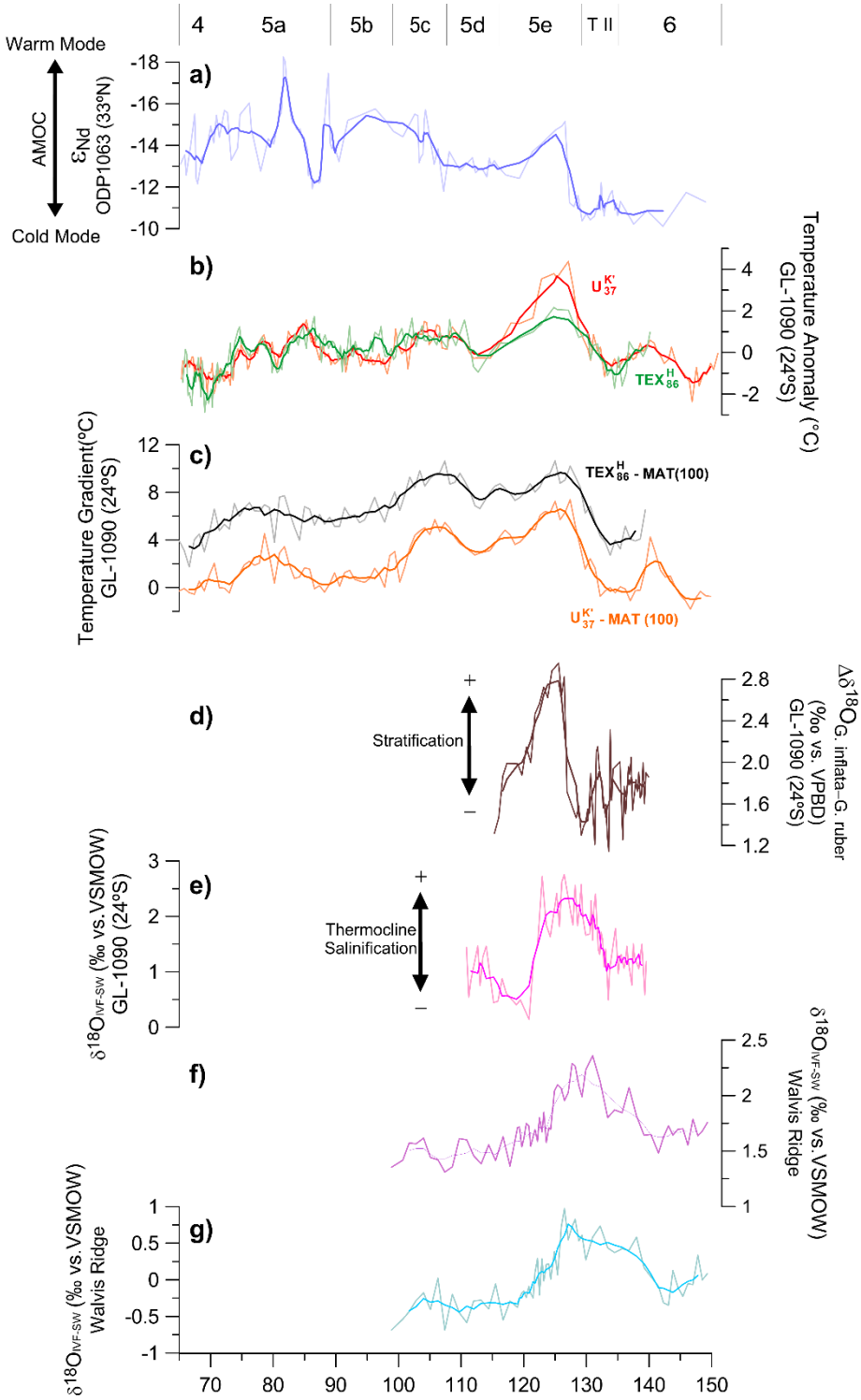

Figure 7: Comparison of temperature anomalies from core GL-1090 with other low/mid-paleoclimate signals from 150 to 65 ka: a) εNd record of core ODP1063 (Böhm et al., 2015); b) Temperature anomalies from core GL-1090 based on TEX_{86}^{H} (green) and $U_{37}^{K'}$ (red) (this study); c) Temperature gradient from core GL-1090 based on TEX_{86}^{H} (this study) minus MAT-100m (Lessa et al., 2017; green), and $U_{37}^{K'}$ (this study) minus MAT-100m (Lessa et al., 2017; red); d) $\Delta\delta^{18}O$ (*Globorotalia inflata – Globigerinoides ruber*) (Santos et al.,

2017); e) Thermocline $\delta^{18}O_{IVC\text{-}SW}$ values from core GL-1090 (Ballalai et al., 2019) estimated from Mg/Ca ratio-derived thermocline temperatures; f) Surface $\delta^{18}O_{IVC\text{-}SW}$ values from core 64PE- 174P13 (Walvis Ridge) (Scussolini et al., 2015) estimated from *Globigerinoides ruber* $\delta^{18}O$ values; g) Thermocline $\delta^{18}O_{IVC\text{-}SW}$ values from core 64PE-174P13 (Walvis Ridge) (Scussolini et al., 2015) estimated from *Globigerinoides truncatulinoides* $\delta^{18}O$ values. Marine isotope stages (MIS) are highlighted on the upper x-axis. (For interpretation of the references to color in this figure legend, the reader is referred to the web version of this article.)

Furthermore, during MIS 5e and MIS 5c, the high ΔT between the organic proxies $U^{K'}_{37}/TEX^{H}_{86}$ and MAT-100 (Fig. 7) suggests upper ocean stratification with the flattening of the mixed layer, which may have reduced the downward diffusion of heat. This decrease in vertical mixing due to enhanced stratification is showed by $\Delta\delta^{18}O$ (*G. inflata* - *G. ruber*) (Fig. 7d). Leonhardt et al. (2013) analyzed fossil assemblages of coccolithophorids, *Globigerinoides ruber* and corresponding stable oxygen isotopes from a sediment core collected in the SSWA, covering the last 130 ka. The authors observed lower surface productivity during MIS 5e, which was related to an increase in the nutricline depth, making surface water fertilization impossible.

During late MIS 6 / T II and the onset of MIS 4, sea temperature positive anomalies (Fig. 7b) were associated with the weakening of the AMOC and consequent strengthening of the BC due to changes in circulation structure (Broecker, 1998; Santos et al., 2017). The εNd, a water mass provenance proxy used for interpretation of water mass geometry from the Bermuda Rise (Böhm et al., 2015), corroborates this hypothesis (Fig. 7a).

It is known that warm and saline Subtropical Indian Ocean water is transported into the South Atlantic through the Indian-Atlantic oceanic gateway (Gordon, 1986; Lutjeharms, 2006; Beal et al., 2011). Marino et al. (2013) point that the salinity increase between 138 ka and 130 ka indicated by $\delta^{18}O_{SW}$ represents an interhemispheric coupling

once it is correlated with abrupt swings in the North Atlantic. According to Marino et al. (2013), the Indian-to-Atlantic salt transport is a strong driver of the AMOC during the abrupt climate changes of the Late Pleistocene.

Ballalai et al. (2019) analyzed thermocline Mg/Ca-derived temperatures and salinity from ice volume-corrected $\delta^{18}O$ seawater ($\delta^{18}O_{IVC\text{-}SW}$) records in GL-1090 during Termination II and early Late Interglacial (Fig. 7e). According to these authors, during the intensification of the Agulhas Leakage, starting from ca. 142 ka BP (Fig. 7f; g), the salt anomaly was recirculated within the South Atlantic subtropical gyre instead of being immediately transmitted to the North Atlantic due to a "barrier" caused by an ocean-atmosphere coupling that increased the BC flow and limited its equatorial crossing. Our findings are consistent with those of Ballalai et al. (2019). In this sense, this study confirm the connection between the intensification of the Agulhas Leakage and the heat storage at the upper thermocline in the SSWA during MIS 5e.

In summary, our organic data from GL-1090 provided information on the applicability of the $U^{K'}_{37}$ and TEX^{H}_{86} proxies in the SSWA and have enabled the identification of a change in the thermocline structure in the SSWA from late MIS 6 to the onset of MIS 4. Based on our results, we suggest that alkenones were more affected by warm temperatures at the upper thermocline during the LIG period (MIS 5e), and isoGDGTs were more affected by cold temperatures at the mixed layer during glacials (MIS 6 and MIS 4). However, more studies covering the same time range with atmospheric modeling and thermocline proxies in the South Atlantic must be considered in future research studies in the region in order to better understand the mechanisms that led to these scenarios.

6. CONCLUSIONS

This work presents the first temperature reconstruction based on alkenones and isoGDGTs covering late MIS 6 to the onset of MIS 4 in the SSWA. A multiproxy approach was developed, involving the organic proxies $U^{K'}_{37}$ and TEX^{H}_{86}, as well as previously published data (Mg/Ca ratio and MAT derived from planktonic foraminifera). Non-thermal factors, i.e. terrestrial inputs and lateral transport, were suggested to have minor influence on the temperature signal derived from alkenones/isoGDGTs. TEX^{H}_{86} and $U^{K'}_{37}$ temperature estimates were assumed to reflect different water depths, i.e. those of the mixed layer and the upper thermocline, respectively. This was related to the different habitat depths of the source organisms of isoGDGTs and alkenones - marine *Thaumarchaeota* and hapophyte algae, respectively.

Our downcore record emphasizes the relevance of a multiproxy approach to bringing insights into the interpretation of the response of each proxy in the same sediment core, leading to better understanding of the paleoceanographic changes from 150 ka to 65 ka, mainly during the LIG, in the south-eastern Brazilian margin. Our results suggest that a steep thermal gradient in the upper thermocline exists during the LIG, as does a reduced thermal gradient in the glacial scenario. Finally, our study demonstrates that the organic proxies applied here are reliable for reconstructing paleoceanographic changes in the SSWA.

CRediT AUTHORSHIP CONTRIBUTION STATEMENT

Joana F. Cruz: writing – original draft, formal analysis, conceptualization. Alice M. S. Rodrigues, Thiago P. Santos, Igor M. Venancio, Douglas Lessa, Rodrigo L. Sobrinho, Rodrigo A. Nascimento: writing – review & editing. Ioanna Bouloubassi, Arnaud Huguet: formal analysis, review & editing. Marcelo C. Bernardes: supervision, formal analysis, review & editing.

DECLARATION OF COMPETING INTEREST

The authors declare that they have no known competing financial interests or personal relationships that could have appeared to influence the work reported in this paper.

ACKNOWLEDGEMENTS

We thank Petrobras for providing the sediment core used in this research, and Vincent Klein (LOCEAN-Sorbonne Université) and Christelle Anquetil (METIS-Sorbonne Université) for their support during the analyses. This study was supported by CAPES/Paleoceano Project (23038.001417/2014-7), CAPES-IODP/Aspecto Project (88887.091731/2014-01), Project CLIMATE/Print-CAPES (88887.310301/2018-00) and Finance Code 001, INSU-CNRS program LEFE (BARISTA project) and partially by CNPq Project 429767/2018-8. Joana F. Cruz thank for her CNPq (140443/2016-9) and CAPES/Programas Estratégicos (88881.145911/2017-01) support. This study was financed in part by CNPq Project RAiN (grant 406322/2018-0). This study was also funded by FAPERJ (SEI-260003/000677/2023), which currently financially supports Igor M. Venancio with a JCNE grant (200.120/2023 – 281226).

REFERENCES

Andruleit, H., Stager, S., Rogalla, U., Cepek, P., 2003. Living coccolithophores in the northern Arabian Sea: ecological tolerances and environmental control, Mar. Micropaleontol., 49, 157-181, https://doi.org/10.1016/S0377-8398(03)00049-5.

Auderset, A., Martínez-García, A., Tiedemann, R., Hasenfratz, A.P., Eglinton, T.I., Schiebel, R., Sigman, D.M., Haug, G.H., 2019. Gulf Stream intensification after the early

Pliocene shoaling of the Central American Seaway, Earth Planet. Sci. Lett., 520, 268–278, https://doi.org/10.1016/j.epsl.2019.05.022.

Ausín, B., Magill, C., Haghipour, N., Fernández, Á., Wacker, L., Hodell, D., Baumann, K.-H., Eglinton, T.I., 2019. (In)coherent multiproxy signals in marine sediments: Implications for high-resolution paleoclimate reconstruction, Earth Planet. Sci. Lett., 515, 38–46, https://doi.org/10.1016/j.epsl.2019.03.003.

Ballalai, J.M., Santos, T.P., Lessa, D.O., Venancio, I.M., Chiessi, C.M., Johnstone, H.J.H., Kuhnert, H., Claudio, M.R., Toledo, F., Costa, K.B., Albuquerque, A.L.S. 2019. Tracking spread of the Agulhas leakage into the western South atlantic and its northward transmission during the last interglacial. Paleoceanog. and Paleoclimatol., [s. l.], v. 34, n. 11, p. 1744-1760, doi: 10.1029/2019PA003653.

Bazin, L., Landais, A., Lemieux-Dudon, B., Toyé Mahamadou Kele, H., Veres, D., Parrenin, F., Martinerie, P., Ritz, C., Capron, E., Lipenkov, V.Y., Loutre, M.-F.; Raynaud, D., Vinther, B.M., Svensson, A.M., Rasmussen, S.O., Severi, M., Blunier, T., Leuenberger, M.C., Fischer, H., Masson-Delmotte, V., Chappellaz, J.A., Wolff, E.W. 2013. An optimized multi-proxy, multi-site Antarctic ice and gas orbital chronology (AICC2012): 120-800 ka. Climate of the Past, [s. l.], v. 9, n. 4, 1715-1731, https://doi.org/10.5194/cp-9-1715-2013.

Beal, L.M., De Ruijter, W.P.M., Biastoch, A., Zahn, R., 2011. On the role of the Agulhas system in ocean circulation and climate, Nature, 472 (7344), 429–436., https://doi.org/10.1038/nature09983.

Benthien, A., Müller, P.J., 2000. Anomalously low alkenone temperatures caused by lateral particle and sediment transport in the Malvinas Current region, western Argentine

Basin, Deep-Sea Res. Part I Oceanogr. Res. Pap., 47, 2369–2393, https://doi.org/10.1016/S0967-0637(00)00030-3.

Blaauw, M., Christeny, J.A., 2011. Flexible paleoclimate age-depth models using an autoregressive gamma process, Bayesian Anal., 6, 457–474, doi:10.1214/11-BA618.

Böhm, E.; Lippold, J.; Gutjahr, M.; et al, 2015. Strong and deep Atlantic meridional overturning circulation during the last glacial cycle. Nature, v. 517, n. 7534, p. 73–76.

Brandini, F.P., Nogueira Jr, M., Simião, M., Codina, J.C.U., Noernberg, M.A., 2014. Deep chlorophyll maximum and plankton community response to oceanic bottom intrusions on the continental shelf in the South Brazilian Bight, Cont. Shelf Res., 89, 61–75, https://doi.org/10.1016/j.csr.2013.08.002.

Brassell, S.C., Eglinton, G., Marlowe, I.T., Pflaumann, U., Sarnthein, M., 1986. Molecular stratigraphy: a new tool for climatic assessment, Nature, 320, 129–133, https://doi.org/10.1038/320129a0.

Campos, E.J.D., Miller, J.L., Moiler, T.J., Peterson, R.G., 1995. Physical oceanography of the Southwest Atlantic Ocean, Oceanography, 8, 87-91, https://doi.org/10.5670/oceanog.1995.03.

Campos, E.J.D., Velhote, D., Silveira, I.C.A., 2000. Shelf break upwelling driven by Brazil current cyclonic meanders, Geophys. Res. Lett., 27, 751-754, https://doi.org/10.1029/1999GL010502.

Capron, E., Govin, A., Stone, E.J., Masson-Delmotte, V., Mulitza, S., Otto-Bliesner, B., Rasmussen, T.L., Sime, L.C., Waelbroeck, C., Wolff, E.W., 2014. Temporal and spatial structure of multi-millennial temperature changes at high latitudes during the Last

Interglacial, Quat. Sci. Rev., 103, 116-133, https://doi.org/10.1016/j.quascirev.2014.08.018.

Ceccopieri, M., Carreira, R.S., Wagener, A.L.R., Hefter, J., Mollenhauer, G., 2018. On the application of alkenone- and GDGT-based temperature proxies in the southeastern Brazilian continental margin, Org. Geochem., 126, 43-56, https://doi.org/10.1016/j.orggeochem.2018.10.009.

Chiessi, C.M., Ulrich, S., Mulitza, S., Pätzold, J., Wefer, G., 2007. Signature of the Brazil-Malvinas Confluence (Argentine Basin) in the isotopic composition of planktonic foraminifera from surface sediments. Mar. Micropaleontol., 64, 1–2, 52–66, https://doi.org/10.1016/j.marmicro.2007.02.002.

Chiessi, C.M., Mulitza, S., Groeneveld, J., Silva, J.B., Campos, M.C., Gurgel, M.H.C., 2014. Variability of the Brazil Current during the late Holocene. Palaeogeogr. Palaeoclimatol. Palaeoecol., 415, 28–36, http://dx.doi.org/10.1016/j.palaeo.2013.12.005.

Chiessi, C.M., Mulitza, S., Mollenhauer, G., Silva, J.B., Groeneveld, J., Prange, M., 2015. Thermal evolution of the western South Atlantic and the adjacent continent during Termination 1, Clim. Past, 11, 915–929, https://doi.org/10.5194/cp-11-915-2015.

Conti, L.A., Furtado, V.V., 2006. Geomorfologia da Plataforma Continental do Estado de São Paulo, Braz. J. Geol., 36 (2): 305-312.

Costa, K.B.; Cabarcos, E.; Santarosa, A.C.A.; Battaglin, B.B.F.; Toledo, F.A.L., 2016. A multiproxy approach to the climate and marine productivity variations along MIS 5 in SE Brazil: A comparison between major components of calcareous nannofossil assemblages and geochemical records. Palaeogeography, Palaeoclimatology, Palaeoecology, Amsterdam, v. 449, p. 275–288.

Cordeiro, L.G.M.S., Belem, A.L., Bouloubassi, I., Rangel, B., Sifeddine, A., Capilla, R., Albuquerque, A.L.S., 2014. Reconstruction of southwestern Atlantic sea surface temperatures during the last Century: Cabo Frio continental shelf (Brazil), Palaeogeogr. Palaeoclimatol. Palaeoecol., 415, 225–232, https://doi.org/10.1016/j.palaeo.2014.01.020.

Crampton-Flood, E.D., Peterse, F., Sinninghe Damsté, J.S., 2019. Production of branched tetraethers in the marine realm: Svalbard fjord sediments revisited, Org. Geochem., 138, 103907, https://doi.org/10.1016/j.orggeochem.2019.103907.

Dauner, A.L.L., Mollenhauer, G., Bícego, M.C., de Souza, M.M., Nagai, R.H., Figueira, R.C.L., Mahiques, M.M., de Melo e Souza, S.H., Martins, C.C., 2019. Multi-proxy reconstruction of sea surface and subsurface temperatures in the western South Atlantic over the last ~75 kyr. Quat. Sci. Rev., 215, 22–34. https://doi.org/10.1016/j.quascirev.2019.04.020.

Evangelista, H., Gurgel, M., Sifeddine, A., Rigozo, N.R., Boussafir, M., 2014. South Tropical Atlantic anti-phase response to Holocene Bond Events, Palaeogeogr. Palaeoclimatol. Palaeoecol., 415, 21–27, https://doi.org/10.1016/j.palaeo.2014.07.019.

Figueiredo, T.S., Santos, T.P., Costa, K.B., Toledo, F., Albuquerque, A.L.S., Smoak, J.M., Bergquist, B.A., Silva-Filho, E.V., 2020. Effect of deep Southwestern Subtropical Atlantic Ocean circulation on the biogeochemistry of mercury during the last two glacial/interglacial cycles, Quat. Sci. Rev., 239, 106368, https://doi.org/10.1016/j.quascirev.2020.106368.

Gordon, A.L., 1986. Inter-ocean exchange of thermocline water, J. Geophys. Res., 91(C4), 5037‑5046.

Govin, A., Chiessi, C.M. , Zabel, M., Sawakuchi, A.O., Heslop, D., Hörner, T., Zhang, Y., Mulitza, S., 2014. Terrigenous input off northern South America driven by changes in Amazonian climate and the North Brazil Current retroflection during the last 250 ka, Clim. Past, 10, 2, 843–862, http://dx.doi.org/10.5194/cp-10-843-2014.

Govin, A., Capron, E., Tzedakis, P.C., Verheyden, S., Ghaleb, B., Hillaire-Marcel, C., St-Onge, G., Stoner, J.S., Bassinot, F., Bazin, L., Blunier, T., Combourieu-Nebout, N., El Ouahabi, A., Genty, D., Gersonde, R., Jimenez-Amat, P., Landais, A., Martrat, B., Masson-Delmotte, V., Parrenin, F., Seidenkrantz, M.S., Veres, D., Waelbroeck, C., Zahn, R., 2015. Sequence of events from the onset to the demise of the Last Interglacial: Evaluating strengths and limitations of chronologies used in climatic archives, Quat. Sci. Rev., 129, 1–36, http://doi.org/10.1016/j.quascirev.2015.09.018.

Gray, W.R., Evans, D. 2019. Nonthermal influences on Mg/Ca in planktonic foraminifera: a review of culture studies and application to the last glacial maximum. Paleoceanography and Paleoclimatology, [s. l.], v. 34, p. 306-315, https://doi.org/10.1029/2018PA003517.

Hansen, J., Sato, M., Hearty, P., Ruedy, R., Kelley, M., Masson-Delmotte, V., Russell, G., Tselioudis, G., Cao, J., Rignot, E., Velicogna, I., Tormey, B., Donovan, B., Kandiano, E., von Schuckmann, K., Kharecha, P., Legrande, A.N., Bauer, M., Lo, K.-W., 2016. Ice melt, sea level rise and superstorms: evidence from paleoclimate data, climate modeling, and modern observations that 2.0 °C global warming could be dangerous, Atmos. Chem. Phys., 16, 3761–3812, https://doi.org/10.5194/acp-16-3761-2016.

Hoffman, J.S., Clark, P.U., Parnell, A.C., He, F. 2017. Regional and global sea-surface temperatures during the last interglaciation. Science, [s. l.], v. 355, p. 276- 279.

Hopmans, E.C., Weijers, J.W.H., Schefuß, E., Herfort, L., Sinninghe Damsté, J.S., Schouten, S., 2004. A novel proxy for terrestrial organic matter in sediments based on branched and isoprenoid tetraether lipids, Earth Planet. Sci. Lett., 224, 107–116, https://doi.org/10.1016/j.epsl.2004.05.012.

Huguet, A., Fosse, C., Laggoun-Défarge, F., Delarue, F., Derenne, S., 2013. Effects of a short-term experimental microclimate warming on the abundance and distribution of branched GDGTs in a French peatland, Geochim. Cosmochim. Acta., 105, 294-315, https://doi.org/10.1016/j.gca.2012.11.037.

Huguet, A., Coffinet, S., Roussel, A., Gayraud F., Anquetil, C., Bergonzini, L., Bonanomi, G., Williamson, D., Majule A., Derenne, S., 2019. Evaluation of 3-hydroxy fatty acids as a pH and temperature proxy in soils from temperate and tropical altitudinal gradients, Org. Geochem., 129, 1-13, https://doi.org/10.1016/j.orggeochem.2019.01.002.

Huguet, C., Martrat, B., Grimalt, J.O., Sinninghe Damsté, J.S., Schouten, S., 2011. Coherent millennial-scale patterns in $U_{37}^{K'}$ and TEX_{86}^{H} temperature records during the penultimate interglacial-to-glacial cycle in the western Mediterranean, Paleoceanography, 26, PA2218, https://doi.org/10.1029/2010PA002048.

Kim, J.H., van der Meer, J., Schouten, S., Helmke, P.,Willmott, V., Sangiorgi, F., Koç, N., Hopmans, E.C., Sinninghe Damste, J.S., 2010. New indices and calibrations derived from the distribution of crenarchaeal isoprenoid tetraether lipids: implications for past sea surface temperature reconstructions, Geochim. Cosmochim. Acta, 74, 4639-4654, https://doi.org/10.1016/j.gca.2010.05.027.

Kim, J., Romero, O.E., Lohmann, G., Donner, B., Laepple, T., Haam, E., Sinninghe Damsté, J.S., 2012. Pronounced subsurface cooling of North Atlantic waters off

Northwest Africa during Dansgaard-Oeschger interstadials. Earth Planet. Sci. Lett., 340, 95–102, doi: 10.1016/j.epsl.2012.05.018.

Leduc, G., Schneide, R., Kim, J.-H., Lohmann, G., 2010. Holocene and Eemian sea surface temperature trends as revealed by alkenone and Mg/Ca paleothermometry, Quat. Sci. Rev., 29, 989–1004, https://doi.org/10.1016/j.quascirev.2010.01.004.

Leininger, S., T. Urich, M. Schloter, L. Schwark, J. Qi, G. Nicol, J. Prosser, S. Schuster, and C. Schleper, 2006. Archaea predominate among ammonia- oxidizing prokaryotes in soils, Nature, 442, 806–809, doi:10.1038/nature04983.

Leonhardt, A., Toledo, F.A.L., Coimbra, J.C., 2013. The productivity history in the southwestern atlantic as inferred from coccolithophore record for the last 130 kyr, Rev. bras. paleontol. 16(3):361-374.

Lessa, D.V.O., Ramos, R.P., Barbosa, C.F., da Silva, A.R., Belem, A., Turcq, B., Albuquerque, A.L.S., 2014. Planktonic foraminifera in the sediment of a western boundary upwelling system off Cabo Frio, Brazil, Mar. Micropaleontol., 106, 55–68, https://doi.org/10.1016/j.marmicro.2013.12.003.

Lessa, D.V.O., Venancio, I.M., dos Santos, T.P., Belem, A.L., Turcq, B.J., Sifeddine, A., Albuquerque, A.L.S., 2016. Holocene oscillations of Southwest Atlantic shelf circulation based on planktonic foraminifera from an upwelling system (off Cabo Frio, Southeastern Brazil), The Holocene, 26, 1175–1187, https://doi.org/10.1177/0959683616638433.

Lessa, D.V.O., Santos, T.P., Venancio, I.M., Albuquerque, A.L.S., 2017. Offshore expansion of the Brazilian coastal upwelling zones during Marine Isotope Stage 5, Glob. Planet. Change, 158, 13–20, https://doi.org/10.1016/j.gloplacha.2017.09.006.

Lisiecki, L.E., Raymo, M.E., 2005. A Pliocene-Pleistocene stack of 57 globally distributed benthic $\delta^{18}O$ records, Paleoceanography, 20, 1, 1–17, https://doi.org/10.1029/2004PA001071.

Locarnini, R.A., Mishonov, A.V., Antonov, J.I., Boyer, T.P., Garcia, H.E., Baranova, O.K., Zweng, M.M., Paver, C.R., Reagan, J.R., Johnson, D.R., Hamilton, M., Seidov, D., 2013. World Ocean Atlas 2013, Volume 1: Temperature. NOAA Atlas NESDIS.

Lopes dos Santos, R.A., Spooner, M.I., Barrows, T.T., De Deckker, P., Sinninghe Damsté, J.S., Schouten, S., 2013. Comparison of organic ($U^{K'}_{37}$, TEX^{H}_{86}, LDI) and faunal proxies (foraminiferal assemblages) for reconstruction of late Quaternary sea surface temperature variability from offshore southeastern Australia, Paleoceanography, 28, 377–387, https://doi.org/10.1002/palo.20035.

Lourenço, R.A., Mahiques, M.M., Wainer, I.E.K.C., Rosell-Melé, A., Bícego, M.C., 2016. Organic biomarker records spanning the last 34,800 years from the southeastern Brazilian upper slope: links between sea surface temperature, displacement of the Brazil Current, and marine productivity, Geo Mar. Lett., 36, 361-369, https://doi.org/10.1007/s00367-016-0453-7.

Lutjeharms, J.R.E., 2006. The Agulhas Current, 329 pp., Springer, Berlin.

Luz, L.G., Santos, T.P., Eglinton, T.I., Montluçon, D., Ausin, B., Haghipour, N., Sousa, S.M., Nagai, R.H., Carreira, R.S., 2020. Contrasting late-glacial paleoceanographic evolution between the upper and lower continental slope of the western South Atlantic. Climate of the Past, [s. l.], v. 16, p. 1245-1261.

Luz, L.G., 2019. Mudanças oceanográficas e climáticas nos últimos 50 mil anos no sudoeste do Atlântico com base em registros de paleo-indicadores orgânicos e

inorgânicos na Margem Continental do Rio de Janeiro, Brasil. 188 f. Thesis (PhD in Chemistry) - Pontifícia Universidade Católica do Rio de Janeiro, Rio de Janeiro, Brazil.

Mahiques, M.M., Silveira, I.C.A., Sousa, S.H.M., Fukumoto, M.M., 2005. Modern sedimentation in the Cabo Frio upwelling system, An. Acad. Bras. Ciênc., 77, 535–548, http://dx.doi.org/10.1590/S0001-37652005000300013.

Mahiques, M.M., Coaracy Wainer, I.K., Burone, L., Nagai, R., Sousa, S.H.M., Figueira, R.C.L., Silveira, I.C.A., Bícego, M.C., Pavani, V.A.D., Hammer, Ø. 2009. A high-resolution Holocene record on the Southern Brazilian shelf: Paleoenvironmental implications. Quaternary International, [s. l.], v. 206, n. 1–2, p. 52-61.

Mann, M., Bradley, R., Hughes, M., 1998. Global-Scale Temperature Patterns and Climate Forcing Over the Past Six Centuries, Nature, 392, 779-787, https://doi.org/10.1038/33859.

Marino, G., Zahn, R., Ziegler, M., Purcell, C., Knorr, G., Hall, I. R., Ziveri, P., Elderfield, H., 2013. Agulhas salt-leakage oscillations during abrupt climate changes of the Late Pleistocene, Paleoceanography, 28, 599–606, doi:10.1002/palo.20038.

Mathias, G. L., Roud, S. C., Chiessi, C. M., Campos, M. C., Dias, B. B., Santos, T. P., et al., 2021. A multiproxy approach to unravel late Pleistocene sediment flux and bottom water conditions in the western South Atlantic Ocean. Paleoceanography and Paleoclimatology, 36, e2020PA004058. https://doi.org/10.1029/2020PA004058.

Mollenhauer, G., Inthorn, M., Vogt, T., Zabel, M., Sinninghe Damsté, J.S., Eglinton, T.I., 2007. Aging of marine organic matter during cross-shelf lateral transport in the Benguela upwelling system revealed by compound-specific radiocarbon dating. Geochemistry, Geophysics, Geosystems 8, Q09004, doi:10.1029/2007GC001603.

Müller, P.J., Kirst, G., Ruhland, G., von Storch, I., Rosell-Melé, A., 1998. Calibration of the alkenone paleotemperature index $U_{37}^{K'}$ based on core-tops from the eastern South Atlantic and the global ocean (60 °N – 60 °S), Geochim. Cosmochim. Acta, 62, 1757–1772, https://doi.org/10.1016/S0016-7037(98)00097-0.

Otto-Bliesner, B.L., Rosenbloom, N., Stone, E.J., Mckay, N.P., Lunt, D.J., Brady, E.C., Overpeck, J.T. 2013. How warm was the last interglacial? New model–data comparisons. Philosophical Transactions of the Royal Society A, London, v. 371, 20130097, doi: 10.1098/rsta.2013.0097.

Otto-Bliesner, B., Braconnot, P., Harrison, S.P., Lunt, D.J., Abe-Ouchi, A., Albani, S., Bartlein, P., Capron, E., Carlson, A., Dutton, A., Fischer, H., Goelzer, H., Govin, A., Haywood, A., Joos, F., LeGrande, A., Lipscomb, W., Lohmann, G., Mahowald, N., Nehrbass-Ahles, C., Peterschmitt, J.Y., Pausata, F.S.-R., Phipps, S., Renssen, H., 2016. Two Interglacials: Scientific Objectives and Experimental Designs for CMIP6 and PMIP4 Holocene and Last Interglacial Simulations, Clim. Past Discussions, 1-36, https://doi.org/10.5194/cp-2016-106.

Past Interglacials Working Group of PAGES, 2016. Interglacials of the last 800,000 years, Rev. Geophys., 54, 162–219, doi:10.1002/2015RG000482.

Pereira, L.S., Arz, H.W., Pätzold, J., Portilho-Ramos, R.C., 2018. Productivity evolution in the South Brazilian Bight during the last 40,000 years. Paleoceanogr. Paleocl., 33, https://doi.org/10.1029/2018PA003406.

Pessenda, L.C.R., Vidotto, E., De Oliveira, P.E., Buso, A.A., Cohen, M.C.L., Rossetti, D.F., Ricardi-Branco, F.B., Bendassolli, J.A., 2012. Late Quaternary vegetation and coastal environmental changes at Ilha do Cardoso mangrove, southeastern Brazil,

Palaeogeogr. Palaeoclimatol. Palaeoecol., 363-364, 57-68, https://doi.org/10.1016/j.palaeo.2012.08.014.

Peterse, F., Kim, J.- H., Schouten, S., Kristensen, D.K., Koç, N., Sinninghe Damsté, J. S., 2009. Constraints on the application of the MBT/CBT palaeothermometer at high latitude environments (Svalbard, Norway), Org. Geochem., 40, 692–699, doi:10.1016/j.orggeochem.2009.03.004.

Peterson, R.G., Stramma, L., 1991. Upper-level circulation in the South Atlantic Ocean, Prog. Oceanogr., 26, 1–73, https://doi.org/10.1016/0079-6611(91)90006-8.

Piola, A.R., Matano, R.P., 2001. Brazil and Falklands (Malvinas) currents. In: Steele, J. H., Thorpe, S. A., Turekian, K. K. (Eds.), Ocean Currents: A Derivative of the Encyclopedia of Ocean Sciences, Elsevier Inc., 35-43, https://doi.org/10.1016/B978-0-12-409548-9.10541-X.

Piola, A.R., Campos, E.J.D., Möller Jr., O.O., Charo, M., Martinez, C., 2000. Subtropical Shelf Front off eastern South America, J. Geophys. Res. Ocean., 105, 6565-6578, https://doi.org/10.1029/1999JC000300.

Pivel, M.A.G., Santarosa, A.C.A., Toledo, F.A.L., Costa, K.B., 2013. The Holocene onset in the southwestern South Atlantic, Palaeogeogr. Palaeoclimatol. Palaeoecol., 374, 164–172, https://doi.org/10.1016/j.palaeo.2013.01.014.

Portilho-Ramos, R.C., Ferreira, F., Calado, L., Frontalini, F., Toledo, M.B., 2015. Variability of the upwelling system in the southeastern Brazilian margin for the last 110,000 years, Glob. Planet. Chang., 135, 179–189, https://doi.org/10.1016/j.gloplacha.2015.11.003.

Poulton, A.J., Holligan, P.M., Charalampopoulou, A., Adey, T.R., 2017. Coccolithophore ecology in the tropical and subtropical Atlantic Ocean: New perspectives from the Atlantic meridional transect (AMT) programme, Prog. Oceanogr., 158, 150–170, https://doi.org/10.1016/j.pocean.2017.01.003.

Prahl, F.G.,Wakeham, S.G., 1987. Calibration of unsaturation patterns in long-chain ketone compositions for palaeotemperature assessment, Nature, 330, 367–369, https://doi.org/10.1038/330367a0.

Ribeiro, C.G., Lopes dos Santos, A., Marie, D., Pellizari, V.H., Brandini, F.P., Vaulot, D., 2016. Pico and nanoplankton abundance and carbon stocks along the Brazilian Bight, Peer, J 4, e2587, https://doi.org/10.7717/peerj.2587.

Richardson, P.L., 2007. Agulhas leakage into the Atlantic estimated with subsurface floats and surface drifters, Deep-Sea Res. Part I Oceanogr. Res. Pap., 54, 8, 1361–1389, https://doi.org/10.1016/j.dsr.2007.04.010.

Rodrigues, S.V., Marinho, M.M., Cubas Jonck, C.C., Gonçalves, E.S., Brant, V.F., Paranhos, R., Curbelo, M.P., Falcão, A.P., 2014. Phytoplankton community structures in shelf and oceanic waters off southeast Brazil (20 ° - 25 °S), as determined by pigment signatures, Deep. Res. Part I Oceanogr. Res. Pap., 88, 47-62, http://dx.doi.org/10.1016/j.dsr.2014.03.006.

Santos, T.P., Lessa, D.O., Venancio, I.M., Chiessi, C.M., Mulitza, S., Kuhnert, H., Govin, A., Machado, T., Costa, K.B., Toledo, F., Dias, B.B., Albuquerque, A.L.S., 2017a. Prolonged warming of the Brazil Current precedes deglaciations. Earth Planet. Sci. Lett., 463, 1–12, http://dx.doi.org/10.1016/j.epsl.2017.01.014.

Santos, T.P., Lessa, D.O., Venancio, I.M., Chiessi, C.M., Mulitza, S., Kuhnert, H., Albuquerque, A.L.S., 2017b. The impact of the AMOC resumption in the western South Atlantic thermocline at the onset of the Last Interglacial. Geophys. Res. Lett., 44, 11, 547-554, https://doi.org/10.1002/2017GL074457.

Santos, T.P., Ballalai, J.M., Franco, D.R., Oliveira, R.R., Lessa, D.O., Venancio, I.M., Chiessi, C.M.; Kuhnert, H., Johnstone, H., Albuquerque, A.L.S., 2020. Asymmetric response of the subtropical western South Atlantic thermocline to the Dansgaard-Oeschger events of Marine Isotope Stages 5 and 3. Quat. Sci. Rev., Oxford, v. 237, n. 106307.

Schlitzer, R., 2013. Ocean Data View, http://www.awi- bremerhaven.de/GEO/ODV.

Schmid, C., 2014. Mean vertical and horizontal structure of the subtropical circulation in the South Atlantic from three-dimensional observed velocity fields, Deep. Res. Part I Oceanogr. Res. Pap., 91, 50-71, https://doi.org/10.1016/j.dsr.2014.04.015.

Schouten, S., Hopmans, E.C., Schefuß, E., Sinninghe Damsté, J.S., 2002. Distributional variations in marine crenarchaeol membrane lipids: a new tool for reconstructing ancient sea water temperatures?, Earth Planet. Sci. Lett., 204, 265–274, doi: 10.1016 / S0012-821X (02) 00979-2.

Schouten, S., Hopmans, E.C., Sinninghe Damsté, J.S., 2013. The organic geochemistry of glycerol dialkyl glycerol tetraether lipids: A review. Org. Geochem. 54, 19-61.

Scussolini, P., Marino, G., Brummer, G.- J. A., Peeters, F. J. C., 2015. Saline Indian Ocean waters invaded the South Atlantic thermocline during glacial termination II. Geology, 43(2), 139–142. https://doi.org/10.1130/G36238.1.

Shah, S.R., Mollenhauer, G., Ohkouchi, N., Eglinton, T.I., Pearson, A., 2008. Origins of archaeal tetraether lipids in sediments: Insights from radiocarbon analysis. Geochimica et Cosmochimica Acta 72, 4577–4594.

Silveira, I.C.A., Schmidt, A.C.K., Campos, E.J.D., Godoi, S.S., Ikeda, Y., 2000. A corrente do Brasil ao largo da costa leste brasileira, Rev. Bras. Oceanogr., 48, 171-183, https://doi.org/10.1590/S1413-77392000000200008.

Sinninghe Damsté, J.S., Ossebaar, J., Abbas, B., Schouten, S., Verschuren, D., 2009. Fluxes and distribution of tetraether lipids in an equatorial African lake: Constraints on the application of the TEX86 palaeothermometer and BIT index in lacustrine settings, Geochim. Cosmochim. Acta, 73, 4232–4249, doi:10.1016/j.gca.2009.04.022.

Sousa, S.H.M., De Godoi, S.S., Amaral, P.G.C., Vicente, T.M., Martins, M.V.A., Sorano, M.R.G.S., Mahiques, M.M., 2014. Distribution of living planktonic foraminifera in relation to oceanic processes on the southeastern continental Brazilian margin (23 °S – 25 °S and 40 °W – 44 °W). Continental Shelf Research, Oxford, v. 89, p. 76-87.

Stramma, L., England, M., 1999. On the water masses and mean circulation of the South Atlantic Ocean, J. Geophys. Res. Ocean., 104, 20863–20883, https://doi.org/10.1029/1999JC900139.

Ternois, Y., Sicre, M.A., Boireau, A., Conte, M.H., Eglinton, G., 1997. Evaluation of long-chain alkenones as paleo-temperature indicators in the Mediterranean Sea. Deep-Sea Res. Part I Oceanogr. Res. Pap., 44, 271–286, https://doi.org/10.1029/96PA00041.

Tierney, J.E., Russell, J.M., Eggermont, H., Hopmans, E.C., Verschuren, D., Sinninghe Damsté, J.S., 2010. Environmental controls on branched tetraether lipid distributions in

tropical East African lake sediments, Geochim. Cosmochim. Acta, 74, 4902–4918, doi:10.1016/j.gca.2010.06.002.

Tierney, J. E., Tingley, M., P., 2014. A Bayesian, spatially-varying calibration model for the TEX_{86} proxy, Geochim. Cosmochim. Acta, 127, 83-186, http://dx.doi.org/10.1016/j.gca.2013.11.026.

Tierney, J. E., Tingley, M., P., 2018. BAYSPLINE: A new calibration for the alkenone paleothermometer, Paleoceanography and Paleoclimatology, 33, 281–301, https://doi.org/10.1002/2017PA003201.

Turney, C.S.M., Jones, R.T., 2010. Does the Agulhas Current amplify global temperatures during super-interglacials?, J. Quat. Sci., 25, 6, 839-843, https://doi.org/10.1002/jqs.1423.

Venancio, I.M., Belem, A.L., Lessa D.O., Albuquerque, A.L.S., Mulitza, S., Schulz, M., Kucera, M., 2017. Calcification depths of planktonic foraminifera from the southwestern Atlantic derived from oxygen isotope analyses of sediment trap material, Mar. Micropaleontol., 136, 37–50, https://doi.org/10.1016/j.marmicro.2017.08.006.

Veres, D., Bazin, L., Landais, A., Toyé Mahamadou Kele, H., Lemieux- Dudon, B., Parrenin, F., Martinerie, P., Blayo, E., Blunier, T., Capron, E., Chappellaz, J., Rasmussen, S. O., Severi, M., Svensson, A., Vinther, B., Wolff, E. W., 2013. The Antarctic ice core chronology (AICC2012): an optimized multi- parameter and multi-site dating approach for the last 120 thousand years. Climate of the Past, [s. l.], v. 9, p. 1733–1748, doi:10.5194/cp-9-1733-2013.

Wainer, I., Prado, L.F., Khodri, M., Otto-Bliesner, B., 2014. Reconstruction of the South Atlantic Subtropical Dipole index for the past 12,000 years from surface temperature proxy, Sci. Rep., 4, 5291, https://doi.org/10.1038/srep05291.

Walsh, E.M., Ingalls, A.E., Keil, R.G., 2008. Sources and transport of terrestrial organic matter in Vancouver Island fjords and the Vancouver–Washington Margin: A multiproxy approach using d13Corg, lignin phenols, and the ether lipid BIT index, Limnol. Oceanogr., 53, 1054–1063, doi:10.4319/lo.2008.53.3.1054.

Weijers, J.W.H., Schouten, S., Spaargaren, O.C., Sinninghe Damsté, J.S., 2006. Occurrence and distribution of tetraether membrane lipids in soils: implications for the use of the TEX86 proxy and the BIT index, Org. Geochem., 37, 1680–1693, https://doi.org/10.1016/j.orggeochem.2006.07.018.

Wuchter, C., Schouten, S., Coolen, M.J.L., Sinninghe Damsté, J.S., 2004. Temperature-dependent variation in the distribution of tetraether membrane lipids of marine Crenarchaeota: Implications for TEX86 paleothermometry. Paleoceanography, Washington, v. 19, p. 1–10.

Zubkov, M.V., Sleigh, M.A., Burkill, P.H., Leakey, R.J.G., 2000. Picoplankton community structure on the Atlantic Meridional Transect: a comparison between seasons. Progress in Oceanography, Oxford, v. 45, p. 369-386.

SUPPLEMENTARY MATERIAL

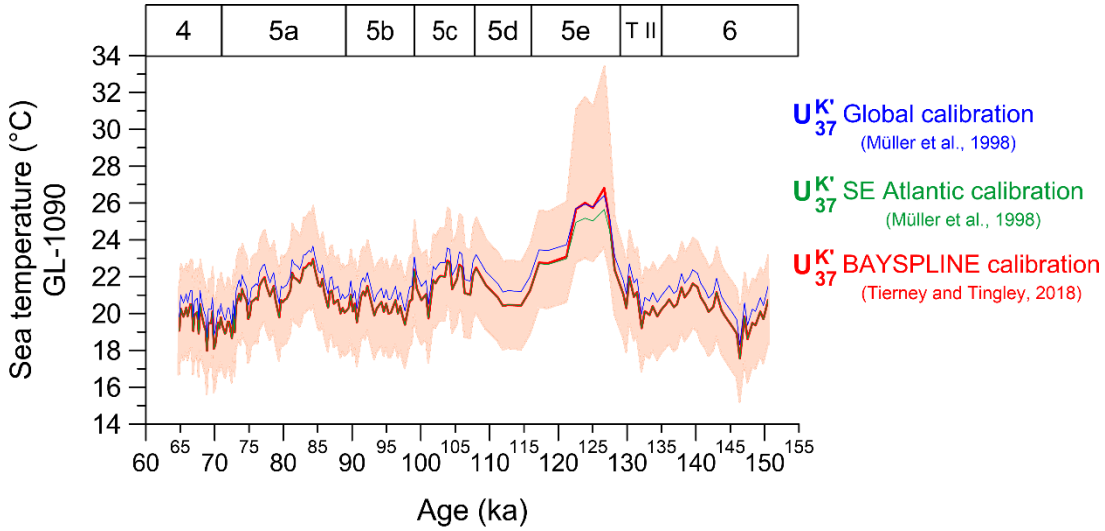

Supp. Fig. 1: Temp-$U^{K'}_{37}$ Global calibration - annual average (Müller et al., 1998) (blue), Temp-$U^{K'}_{37}$ SE Atlantic calibration - annual average (Müller et al., 1998) (green), and Temp-$U^{K'}_{37}$ BAYSPLINE calibration (Tierney and Tingley, 2018) (red) - red shading represents the 95% confidence interval. Marine isotope stages (MIS) are highlighted on the upper x-axis. (For interpretation of the references to color in this figure legend, the reader is referred to the web version of this article.)

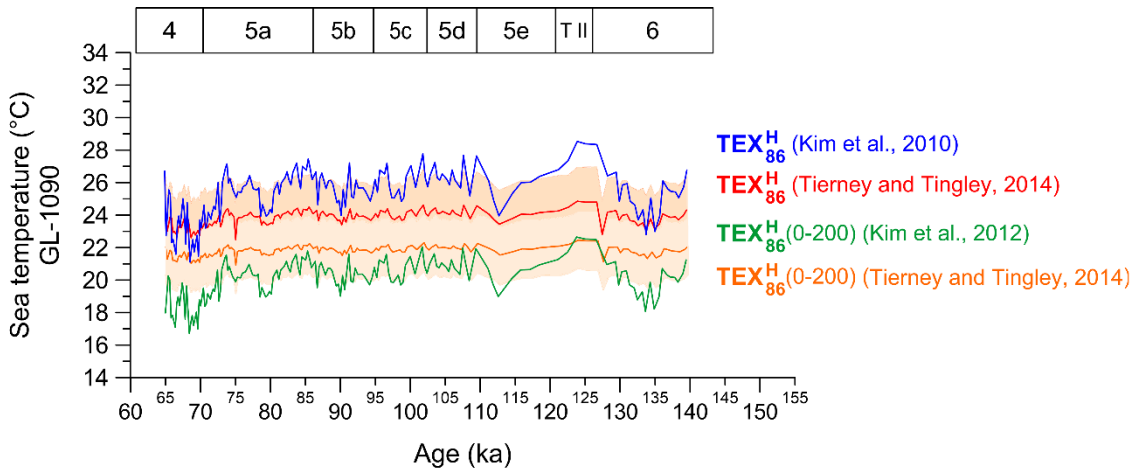

Supp. Fig. 2: Temp-TEX^{H}_{86} Global calibration - annual average (> 15 °C) (Kim et al., 2010) (blue), Temp-TEX^{H}_{86} (0-200) Global calibration - annual average (Kim et al., 2012) (green), Temp-TEX^{H}_{86} Bayesian calibration (Tierney and Tingler, 2014) (red) - red shading

represents the 95% confidence interval, and SubTemp-TEX_{86}^{H} Bayesian calibration (Tierney and Tingler, 2014) (orange) - orange shading represents the 95% confidence interval. Marine isotope stages (MIS) are highlighted on the upper x-axis. (For interpretation of the references to color in this figure legend, the reader is referred to the web version of this article.)

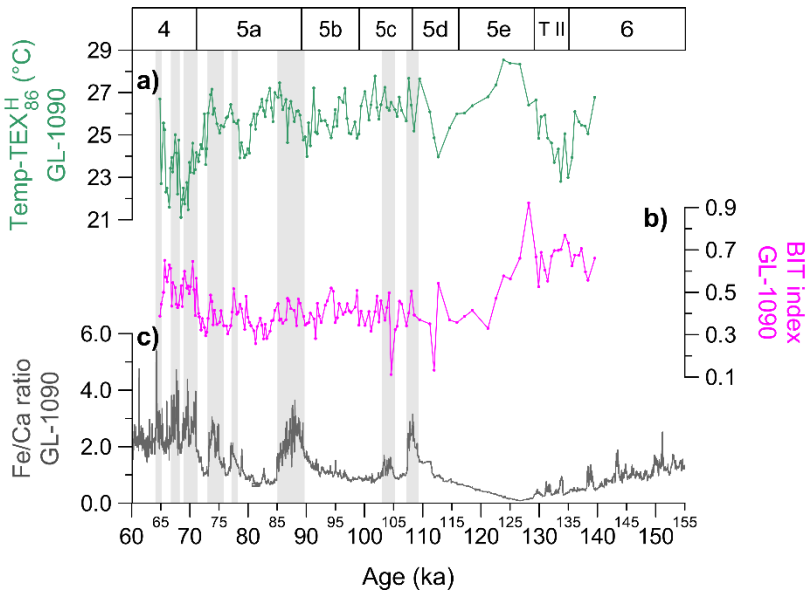

Supp. Fig. 3: Comparison between (a) Temp-TEX_{86}^{H} (green) (this study), (b) BIT index (pink) (this study) and (c) Fe/Ca ratio (gray) (Figueiredo et. al, 2020). Gray bars indicate peaks in Fe/Ca ratios. Marine isotope stages (MIS) are highlighted on the upper x-axis. (For interpretation of the references to color in this figure legend, the reader is referred to the web version of this article.)